

# ‘Hyper Parameters’ Approach to Joint Estimation: Applications to Cepheid-Calibrated Distances and X-Ray Clusters

Pirin Erdogdu<sup>1,2</sup>, Stefano Ettori<sup>3</sup> and Ofer Lahav<sup>1</sup>

<sup>1</sup>Institute of Astronomy, Madingley Road, Cambridge CB3 0HA, UK

<sup>2</sup>Department of Physics, Middle East Technical University, 06531, Ankara, Turkey

<sup>3</sup>ESO, Karl-Schwarzschild-Str. 2, D-85748 Garching bei Munchen, Germany

3 November 2018

## ABSTRACT

We use a generalised procedure for the combined likelihood analysis of different cosmological probes, the ‘Hyper-Parameters’ method, that allows freedom in the relative weights of the raw measurements. We perform a joint analysis of the cepheid-calibrated data from the Hubble Space Telescope Key Project and the baryon mass fraction in clusters to constrain the total matter density of the universe,  $\Omega_m$ , and the Hubble parameter,  $h$ . We compare the results obtained using Hyper-Parameters method with the estimates from standard  $\chi^2$  analysis. We assume that the universe is spatially flat, with a cosmological constant. We adopt the Big-Bang nucleosynthesis constraint for the baryon density, assuming the uncertainty is Gaussian distributed. Using this and the cluster baryon fraction data, we find that the matter density and the Hubble constant are correlated,  $\Omega_m h^{0.5} \approx 0.25$ , with preference for a very high  $h$ . To break the degeneracy, we add in the cepheid-calibrated data and find the best fit values  $(\Omega_m, h) = (0.26^{+0.06}, 0.72^{+0.04})$  (68 per cent confidence limits) using the Hyper-Parameters approach. We use the derived Hyper-Parameters to ‘grade’ the 6 different data sets we analyse. Although our analysis is free of assumptions about the power spectrum of fluctuations, our results are in agreement with the  $\Lambda$ -Cold Dark Matter ‘concordance’ parameters derived from the Cosmic Microwave Background anisotropies combined with Supernovae Ia, redshift surveys and other probes.

**Key words:** cosmology: observations – cosmology:theory – large-scale structure of universe – galaxies: clusters – methods:statistical – X-ray: clusters.

## 1 INTRODUCTION

Combining different cosmological observations has become an essential and common approach in cosmology. A number of groups (e.g. Gawiser & Silk 1998; Webster *et al.* 1998; Lineweaver 1998; Eisenstein, Hu & Tegmark 1999; Efstathiou *et al.* 1999, 2002; Bridle *et al.* 1999, 2001a; Bahcall *et al.* 1999; Lahav *et al.* 2002) investigated a range of cosmological parameters by joint analysis of various cosmic probes, e.g. the Cosmic Microwave Background (CMB), Supernovae Ia (SNIa) and redshift surveys.

It is well known that a simultaneous analysis of different probes is essential in finding tight constraints on the cosmological parameters and breaking the intrinsic degeneracies inherent in any single measurement. While this is true, joint likelihood analyses pose several statistical problems. One of these problems arise when data sets are in disagreement (e.g. Press 1996). In this case, the general approach is to exclude the inconsistent measurements in a somewhat ad-hoc way. A more objective approach to this problem was presented in Lahav *et al.* (2000) and Hobson *et al.* (2002), who generalised the conventional joint analysis by utilizing ‘Hyper Parameters’ (hereafter HPs). The HPs provide a useful diagnostic in determining the relative weight that should be given to each exper-

iment. Thus, this procedure gives an objective understanding as to which measurements are problematic and need further assessment of the random and systematic errors. The formalism for the HPs is given in Appendix B.

In this paper we focus on  $\Omega_m$ , the ratio of matter density to the critical value necessary to close the Universe, and the Hubble parameter,  $H_0 = 100h \text{ km s}^{-1} \text{ Mpc}^{-1}$ . We first consider the measurements separately and then combine them using the HPs method, as well as the conventional  $\chi^2$  analysis. We assume a flat universe,  $\Omega_m + \Omega_\Lambda = 1$ , in agreement with the latest CMB results (e.g. de Bernardis *et al.* 2002). We adopt the Big-Bang nucleosynthesis value for  $\Omega_b h^2$ , where  $\Omega_b$  is the ratio of baryonic matter density to the critical density.

We investigate the Hubble Space Telescope Key Project cepheid-calibrated data (Freedman *et al.* 2001) and estimates of gas mass fraction,  $f_{\text{gas}}$ , in clusters of galaxies obtained from X-ray observations (Ettori & Fabian 1999; Mohr, Mathiesen & Evrard 1999; Allen, Schmidt & Fabian 2002; following the earlier work of White *et al.* 1993). Unlike analyses (e.g. of the CMB and redshift surveys) that assume a power spectrum of fluctuations in a particular scenario of dark matter, we have selected two probes that when

Sample	$h$	Error
36 Supernovae Ia (SNIa)	0.71	$\pm 0.02_r \pm 0.06_s$
21 Tully-Fisher Clusters (TF)	0.71	$\pm 0.03_r \pm 0.07_s$
11 Fundamental Plane Clusters (FP)	0.82	$\pm 0.06_r \pm 0.09_s$
Surface Brightness Fluctuations (SBF) for 6 Clusters	0.70	$\pm 0.05_r \pm 0.06_s$

**Table 1.** The values of  $h$  and the 1-sigma random( $r$ ) and systematic( $s$ ) uncertainties for Cepheid-calibrated samples (from F01, and the references therein)

combined measure  $\Omega_m$  with minimal assumptions, independent of the nature of dark matter. The main assumptions we made in our analysis are as follows: (i) the local  $H_0$  measurements are typical of the entire universe, (ii) the clusters of galaxies are representative of the matter distribution on large scales (but see e.g. Bahcall & Comerford 2002), (iii) all the systematic errors of the measurements are included.

In Sections 2 and 3, we introduce the data and discuss the methods used to produce likelihoods for the individual data sets. We combine the two data sets in Section 4. In Section 5, we discuss our results and compare them with other studies of baryon fraction and independent measurements from the CMB and the 2dF galaxy redshift survey.

## 2 HUBBLE CONSTANT FROM CEPHEID-CALIBRATED DISTANCES

One of the most important results on the Hubble constant comes from the Hubble Space Telescope Key Project (Freedman *et al.* 2001, hereafter F01). The group has used the cepheid period-luminosity relations to obtain distances to 31 galaxies and calibrated a number of secondary distance indicators measured over distances of 400 to 600 Mpc. The values of  $h$  derived using these methods and the uncertainties (random ( $r$ ) and systematic ( $s$ )) are summarised in Table 1. Combining the measurements in Table 1 by several statistical methods they derive the final result as  $h = 0.72 \pm 0.03_r \pm 0.07_s$ . Given the importance of this widely quoted result, we perform a more principled statistical analysis than used by F01 to test robustness of this value.

We use the raw data given in the tables in F01 for Surface Brightness Fluctuations (SBF), SNIa, Tully-Fisher (TF) and Fundamental Plane (FP). We combine these using the standard joint  $\chi^2$  and then the HPs approach. Each method is affected by both systematic errors which are common to all of the methods (e.g. the adopted distance modulus to the Large Magellanic Cloud, metallicity dependence of cepheid period-luminosity relation and reddening by dust) and systematic errors which are specific to each method. In principle, some of systematic errors can be modelled and incorporated in the  $\chi^2$  analysis by adding extra parameters and marginalising over them (for an application to CMB data see Bridle *et al.* 2002). However, we follow F01 and for the variance,  $\sigma^2$ , in the  $\chi^2$  analysis we use the quoted random and systematic errors (from Table 1), added in quadrature. We also test the results when we assume random errors only (see Table 3). In both cases we find the best fit  $h = 0.72$  with the HPs method. This value is in very good agreement with the HST Key project result and also with the standard  $\chi^2$  analysis we performed (Table 2).

The HP values we obtain for each case are given in Table 3. As can be seen from the HPs formalism in Appendix B, the HPs

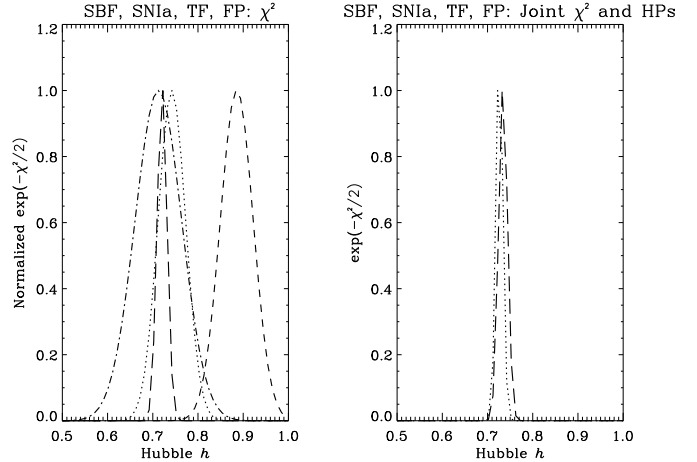


**Figure 1.** Probability functions for the Hubble constant. The left plot shows the  $\chi^2$  statistic for four Cepheid-calibrated distance indicators from F01: SBF(dashed-dotted line), SNIa(long-dashed),TF(dotted) and FP(dashed). The right plot shows the probabilities based on the joint  $\chi^2$  (long-dashed) and the HPs approach (dotted) for the Hubble constant given the same data, with peak values of  $h = 0.72$  and  $h = 0.73$ , respectively. See also Lahav 2001b.

can be interpreted as either an indication of misfit of the data set and the model (e.g. due to systematic problems with the data or to the wrong model), or as a rescaling of the quoted error bars ( $\sigma/\alpha^{1/2}$ ). The HPs scores rank the quality of the methods as follows: SBF (the highest), TF, SNIa and FP. This is in accord with comments on the precision and systematics of each method given by F01. The FP measurements alone give the most discrepant value of  $h$  (Figure 1 and Table 2), and they got the lowest HP (even when the systematic errors were not included in the analysis; see Table 3). This is an example where HPs flag a problem with the measurements. Although the discrepancy of the  $h$  value obtained using FP data alone does not affect the final value derived by joint analyses of FP, SNIa, TF and SBF, one needs to be careful about using the standard  $\chi^2$ . A  $\chi^2$  analysis of discrepant results may lead to a wrong joint answer. A clear example of this problem arises if we use only the FP and the TF data, which have the most similar scatter (see Figure 1) and  $\chi^2$  values (see Table 2) out of all the probes. We find that the joint likelihood function for  $h$  peaks at 0.76 using HPs analysis, whereas the best value of  $h$  is 0.80 using the  $\chi^2$  analysis. In other words, HPs analysis grades the TF measurements as more reliable than the FP data and hence gives the joint value of  $h$  closer to the best value obtained using TF measurements. Using standard joint analysis, the joint likelihood function peaks between the likelihood functions of the two probes, as expected. It is also interesting to note that indeed F01 attached to the FP data the largest systematic errors (see Table 1).

As can be seen in Figure 1, the joint probability functions obtained using the two approaches ( $\chi^2$  and HPs) are both dominated by SNIa data, since SNIa as an indicator possesses the smallest random scatter.

## 3 X-RAY OBSERVATIONS OF CLUSTERS OF GALAXIES

Clusters of galaxies provide various means for the study of the cosmological parameters. Clusters are the largest gravitationally bound structures in the Universe, and therefore generally are assumed to be

Sample	$\chi^2$	Best $h$	68 per cent confidence limits
36 SNIa	19.0	0.72	$0.70 < h < 0.73$
21 TF	7.6	0.74	$0.70 < h < 0.76$
11 FP	4.9	0.88	$0.84 < h < 0.92$
6 SBF	1.7	0.72	$0.66 < h < 0.76$
Joint $\chi^2$ (for 74 data points)	57.0	0.73	$0.70 < h < 0.77$

**Table 2.** The conventional  $\chi^2$  analysis using the raw F01 data. For each sample the best fit value of  $h$  and the  $\chi^2$  value at this point are given.

Sample	HPs (r only)	HPs (r+s)
36 SNIa	0.3	1.9
21 TF	1.9	2.7
11 FP	0.2	0.5
6 SBF	2.8	3.4
Best $h$	0.72	0.72
68 per cent confidence limits	$0.69 < h < 0.76$	$0.68 < h < 0.77$

**Table 3.** The Hyper-parameters analysis using the raw F01 data. For each case the HP is given. The first column is shows the HPs obtained using random errors only, while the second column is for random+systematic errors, added in quadrature.

the tracers of matter distribution on large scales. Provided that  $\Omega_b h^2$ , the baryon density, can be inferred from primordial nucleosynthesis abundance of the light elements, the cluster baryon fraction,  $f_b = \frac{\Omega_b}{\Omega_m}$ , can then be used to constrain  $\Omega_m$  and  $h$  (White *et al.* 1993, Steigman, Hata & Felten 1999, Ettori 2001). The baryons in clusters are primarily in the form of X-ray emitting gas that falls into the cluster halo and secondarily in the form of stellar baryonic mass. Hence the baryon fraction in clusters is estimated to be

$$f_b = \frac{\Omega_b}{\Omega_m} \gtrsim f_{\text{gas}} + f_{\text{gal}}, \quad (1)$$

where  $f_b = M_b/M_{\text{grav}}$ ,  $f_{\text{gas}} = M_{\text{gas}}/M_{\text{grav}}$ ,  $f_{\text{gal}} = M_{\text{gal}}/M_{\text{grav}}$  and  $M_{\text{grav}}$  is the total gravitating mass.

We consider two different datasets of gas mass fraction estimates. The first was published in Ettori and Fabian (1999) (hereafter EF99). This is a sample of 36 relaxed galaxy clusters<sup>\*</sup> with high X-ray luminosities ( $L_x \gtrsim 10^{45} \text{ erg s}^{-1}$ ) and a redshift range from 0.05 to 0.44. The second data set is taken from Mohr, Mathiesen and Evrard (1999) (hereafter MME99). This is an X-ray flux-limited sample of 45 clusters with redshifts between 0.01 and 0.18. Both groups use ROSAT PSPC surface brightness profiles and intercluster medium (ICM) temperatures from ASCA, Ginga and Einstein MPC observations for their analyses. The gas mass fraction estimates,  $f_{\text{gas}}$ , in both datasets are derived assuming the gas is isothermal and in hydrostatic equilibrium within the limiting radius,  $R_\Delta$ , where  $\Delta$  is the mean overdensity of the total mass in a cluster relative to the background value.

<sup>\*</sup> In our analysis, we use 35 clusters instead of 36. Cluster A3888 is excluded from the sample since this cluster's gas temperature was not obtained from X-ray observations but from the gas temperature-optical velocity dispersion relation.

To allow for the variation from cluster to cluster, for the present analysis we use the individual  $f_{\text{gas}}$  per cluster, rather than a global average. As the clusters are at relatively high redshifts,  $f_{\text{gas}}$  is a function of  $\Omega_m$  and  $h$  (see Figure 2). This is due to two cosmological effects (see discussion in, e.g. Ettori 2001).

The first dependence is due to the angular diameter distance,  $d_{\text{ang}}$ , which is a function of  $h$  and  $\Omega_m$  in a flat universe with cosmological constant. For an isothermal gas in hydrostatic equilibrium,  $f_{\text{gas}}$  can be calculated through the surface brightness profile and gas temperature (cf. Ettori & Fabian 1999; Mohr, Mathiesen & Evrard 1999). If the surface brightness profile is measured as the integration of the thermal bremsstrahlung emissivity of the ICM along the line of sight, one finds that  $f_{\text{gas}}$  is proportional to  $d_{\text{ang}}^{1.5}$  (see Appendix A). We calculate the angular diameter distances using Eq. A4 and vary  $h$  and  $\Omega_m$ . We find that  $f_{\text{gas}}$  decreases significantly (about 40 per cent) in a low density universe with  $h > 0.5$ .

The second cosmological dependence is weaker. The hydrodynamical simulations (see e.g. Evrard *et al.* 1996) show that for an Einstein-de Sitter cosmology, a mean overdensity,  $\Delta = 500$  defines a region within  $R_\Delta$  where the assumptions of isothermal gas in hydrostatic equilibrium are valid. Therefore, in both data sets,  $f_{\text{gas}}$  has been estimated at  $\Delta = 500$ . However,  $\Delta$  is function of the cosmological parameters and increases as  $\Omega_m$  decreases in a universe with positive  $\Omega_\Lambda$ .  $R_\Delta$  is proportional to  $(\Omega_m \Delta)^{-0.5}$  (Eq. A7 in Appendix A) and combining this with the radial dependence of the gas mass fraction near  $R_\Delta$  ( $f_{\text{gas}} \propto r^{0.2}$ ), we get  $f_{\text{gas}} \propto (\Omega_m \Delta)^{-0.1}$ . Figure 2 illustrates the dependence of  $f_{\text{gas}}$  on  $h$  and  $\Omega_m$ . We see that  $f_{\text{gas}}$  is mainly sensitive to  $h$ .

We also include the stellar contribution in cluster galaxies,  $f_{\text{gal}}$ , to the baryon fraction estimate. We use a global correction  $f_{\text{gal}} = (0.01 \pm 0.005)h^{-1}$  (Fukugita *et al.* 1998), which is based on mass-to-light ratio,  $M/L = 4.5 \pm 1$  per galaxy, after averaging different galaxy types, with no dependence on  $h$ , hence the  $h$ -dependence in  $f_{\text{gal}}$  comes solely from the  $h$  dependence of  $M_{\text{grav}}$  on the cluster distances. We note that some estimates of  $M/L$  per galaxy depend on the distances to galaxies, and hence on  $h$ , resulting in  $h$ -independent  $f_{\text{gal}}$  (e.g. Wang *et al.* 1999 quote  $f_{\text{gal}} = 0.013$ ). Ideally,  $f_{\text{gal}}$  should be estimated per cluster, but these data are currently unavailable, and in any case it is only a small contribution to the total baryon fraction.

We vary the matter density of the universe in units of the critical density,  $\Omega_m$ , and the present day value of the reduced Hubble constant,  $h$ , over the parameter spaces [0.01, 0.5] and [0.5, 2.5], respectively. We also put a prior on  $\Omega_b h^2$  so that  $\Omega_b h^2 = 0.019 \pm 0.002$ , 95% confidence levels, (e.g. Burles *et al.* 2001) and marginalise over the uncertainty range in order to get the likelihoods of  $\Omega_m$  and  $h$ . We note that fixing  $\Omega_b h^2$  to 0.019 tightens the constraints in the  $\Omega_m$ ,  $h$  plane but does not change the best fit points significantly.

We compute the  $\chi^2$ 's using Eq. B2 in Appendix B:

$$\chi^2 = \sum_i \frac{1}{\sigma_i^2} [f_{b,i}(\Omega_m, h) - \frac{\omega_b}{\Omega_m h^2}]^2, \quad (2)$$

where the sum is over the number of clusters, the baryon fraction is given by  $f_b = f_{\text{gas}} + f_{\text{gal}}$  and  $\omega_b = \Omega_b h^2$ .

To obtain a qualitative understanding we consider Eq. 1 and use the first cosmological dependence that dominates over the others to an approximate relation between  $\Omega_m$  and  $h$ :

$$\Omega_m = \frac{\omega_b h^{-2}}{f_{\text{gas}} + f_{\text{gal}}} \approx \frac{\omega_b h^{-2}}{0.08h^{-1.5} + 0.01h^{-1}}. \quad (3)$$

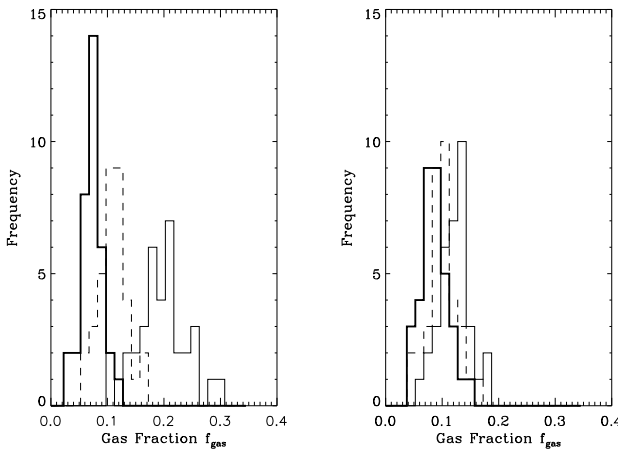


**Figure 2.** The histograms of the gas mass fraction  $f_b$  observed in 35 clusters (EF99). The left panel shows the dependence on  $h$  for fixed  $\Omega_m = 0.3$ :  $h = 0.5$  (solid line),  $h = 0.75$  (dashed line) and  $h = 1.0$  (thick solid line). The right panel shows the dependence on  $\Omega_m$  for fixed  $h = 0.75$ :  $\Omega_m = 0.1$  (solid line),  $\Omega_m = 0.5$  (dashed line) and  $\Omega_m = 1.0$  (thick solid line).

For the observed distribution of the gas mass fraction of about  $0.08 h^{-1.5}$  (e.g. EF99) and reasonable values of Hubble constant, the above relation can be estimated as  $\Omega_m h^{0.5} \approx 0.25$ .

The two datasets do have some clusters in common, however, we see that our conclusions are not affected if we consider the samples separately. The results are plotted in Figure 3. It is seen that in both data sets the value of  $h$  is unacceptably high at the 68% confidence level (but still lower than Hubble's original value of 500 km/sec/Mpc!) and the best fit values of  $\Omega_m$  are relatively low. The parameter values ( $\Omega_m, h$ ) at the best fit points (with 68 per cent confidence limits) are  $(0.11^{+0.03}_{-0.04}, 1.73^{+0.33}_{-0.48})$  and  $(0.18^{+0.02}_{-0.02}, 1.17^{+0.10}_{-0.10})$  for EF99 and MME99 data, respectively. The standard joint analysis of the data sets yields  $(\Omega_m, h) = (0.17^{+0.01}_{-0.02}, 1.23^{+0.08}_{-0.12})$  and with HPs method we obtain  $(\Omega_m, h) = (0.15^{+0.03}_{-0.03}, 1.33^{+0.22}_{-0.28})$ . It is easy to see from Figure 3 that both separate and joint analyses of the data imply that  $\Omega_m = 1$  is ruled out at very high confidence level. The standard  $\chi^2$  and HP analyses, shown on bottom left and right panels in Figure 3 yield slightly different results. The HP values are 0.6 for the EF99 and 0.1 for the MME99 sample. The low weight given to the MME99 data may indicate possible systematic errors, an underestimation of the random errors or incomplete modelling. The HPs obtained suggest that the EF99 sample is more reliable than the MME99 data. The galaxy clusters in the EF99 sample were selected for their high X-ray luminosity and relaxed morphology, whereas the selection criteria in MME99 was to build a flux-limited sample. Therefore, we see at least two effects that can make the EF99 sample more robust in providing a stable central value of the gas fraction: (i) the systematics due to non-homogeneous objects are more under control and (ii) the observed dependence of the value of gas mass fraction upon the plasma temperature (and luminosity, as consequence of the tight  $L - T$  relation observed in galaxy clusters; e.g. Ettori, Allen & Fabian 2001 for an application of HPs to this relation) makes the selection in luminosity (instead of flux) a more robust way to select objects in the upper end of the gas mass fraction distribution.

Being concerned about the high Hubble constant, we applied the Bootstrap method (Efron 1982) to baryon mass fraction data to ensure that there are no outlying clusters which could alter the sig-

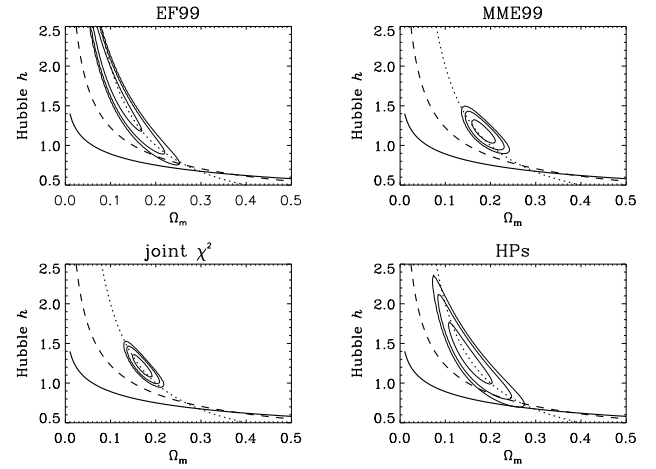


**Figure 3.** The X-ray Cluster Likelihood Functions in the  $\{\Omega_m, h\}$ -plane, after marginalisation over  $\Omega_b h^2$ . The results are compared to estimates from the 2dF Galaxy Redshift Survey:  $\Omega_m h \approx 0.2$  (dashed lines; Percival *et al.* 2001) and from the CMB:  $\Omega_m h^2 \approx 0.15$  (dotted lines; Netterfield *et al.* 2002 and Pryke *et al.* 2002) and the age of the universe  $t_0 \approx 14$  Gyr (solid lines; Knox *et al.* 2001). The contours denote the 68, 95 and 99 percent confidence regions.

nificance of the obtained best fit values. We created 2000 synthetic catalogs selected from the two samples. The histograms of the best fit points for  $h$  and  $\Omega_m$  for these bootstrap realizations are in very good agreement with the presented results.

The joint analysis of cosmological probes (e.g. Bahcall *et al.* 1999 and Efstathiou *et al.* 1999) suggests a flat Universe with  $\Omega_m \approx 0.3$ . We fix  $\Omega_m$  to 0.3 and to 0.2 and plot 1 dimensional likelihood distributions of  $h$ . These plots are shown in Figure 4. For fixed  $\Omega_m = 0.3$  the best fit points of  $h$  are 0.64 and 0.78 for EF99 and MME99, respectively. The joint 1-dimensional likelihood distribution peaks at  $h = 0.72$  using the standard and at  $h = 0.66$  using the HPs approach. Note the good agreement of the best fit value of  $h$  for both data with the F01 result. When  $\Omega_m$  is fixed to be 0.2, the plots shift significantly to the right, with best fit points  $h = 1.03, 1.11, 1.07$  and  $1.03$  for EF99, MME99, standard joint analysis and HPs approach, respectively.

We conclude that the baryon fraction data on its own cannot constrain each of the two parameters, but only their combination,  $\Omega_m h^{0.5} \approx 0.25$ . Therefore, although the likelihood peak is at a high value of  $h$  and a low value of  $\Omega_m$ , we should not attach much significance to the individual values. To constrain the individual values of  $h$  and  $\Omega_m$  we now combine the baryon fraction data with the cepheid sample.

#### 4 COMBINING THE BARYON FRACTION AND THE CEPHEID DATA

We present our results for the combined analysis in Figure 5. It can be seen that the high contour regions obtained for  $h$  with the cluster data have decreased significantly. The confidence regions are a lot tighter than the confidence regions of the single data sets alone, thus giving stronger constraints.

Table 3 and Table 4 show the best fit values and 68% confidence limits of  $h$  and  $\Omega_m$ , respectively. The best fit points of the parameters lie within the confidence limits, indicating that the likelihood distributions are well behaved. The dominating data sets are

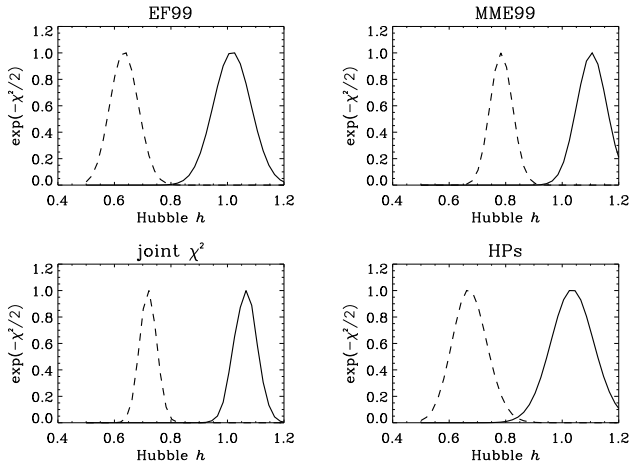


**Figure 4.** The 1-d likelihood distributions of the Hubble Constant for fixed  $\Omega_m = 0.3$  (dashed lines) and  $\Omega_m = 0.2$  (solid lines) and marginalised over  $\Omega_b h^2$ . The figure illustrates that  $h$  is highly sensitive to the assumed  $\Omega_m$ , as  $h$  and  $\Omega_m$  are highly correlated.

Analysis	Best fit value	68 per cent confidence limits
Joint $\chi^2$	0.74	$0.70 < h < 0.78$
HPs	0.72	$0.70 < h < 0.76$

**Table 4.** The values derived for  $h$  using different analysis techniques. The 68% confidence limits are given, calculated for each analysis by marginalising the likelihood function over  $\Omega_b h^2$  and  $\Omega_m$ .

the cepheid-calibrated distance indicators. This is expected, since the uncertainties on  $h$  are much larger for the cluster samples.

The resulting HPs of our analysis are 0.6 (EF99), 0.1 (MME99), 1.8 (SNIA), 2.7 (TF), 0.5 (FP) and 3.3 (SBF). The HPs are actually almost identical to the HPs derived for the individual data sets in section 2 and 3. We also see that the dominance of the cepheid data relative to the baryon fraction data. Since the cepheid data only constrain  $h$ , this leads to a narrower error bar for  $h$  in the HPs analysis compared with the joint  $\chi^2$  (which give equal weight to each of the 6 data sets). Since the cepheid data have no information about  $\Omega_m$  but have higher HP values, the error bar on  $\Omega_m$  is wider in the HPs analysis.

Another interesting result is that the HPs analysis probes a parameter space in good agreement with the results from 2dF Galaxy Survey and CMB anisotropy measurements. The right panel of Figure 5 shows that our combined analysis is consistent with other measurements.

Analysis	Best fit value	68 per cent confidence limits
Joint $\chi^2$	0.25	$0.22 < \Omega_m < 0.29$
HPs	0.26	$0.20 < \Omega_m < 0.32$

**Table 5.** The values derived for  $\Omega_m$  using different analysis techniques. The 68% confidence limits are given, calculated for each analysis by marginalising the likelihood function over  $\Omega_b h^2$  and  $\Omega_m$ .

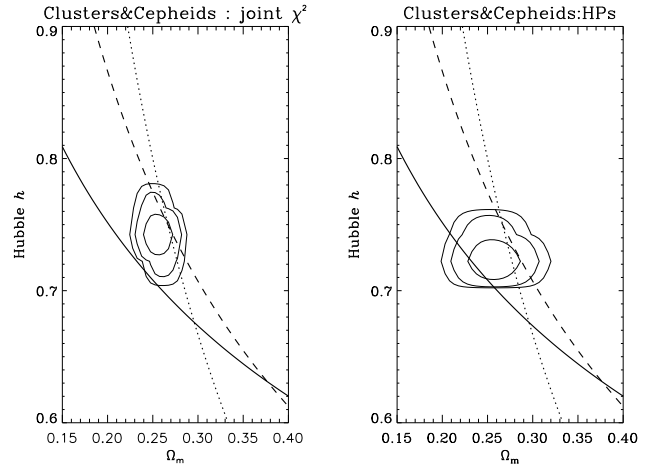


**Figure 5.** The likelihood functions from combining the Cluster data with Cepheids. The results are compared to estimates from the 2dF Galaxy Redshift Survey:  $\Omega_m h \approx 0.2$  (dashed lines) and from the CMB:  $\Omega_m h^2 \approx 0.15$  (dotted lines) and the age of the universe  $t_0 \approx 14$  Gyr (solid lines), as in Figure 3. The contours denote the 68, 95 and 99 percent confidence regions.

## 5 DISCUSSION

We have presented applications of a generalised procedure, 'Hyper-Parameters' (HPs), for analysing a set of different measurements. We performed a combined analysis of baryon fraction in clusters and cepheid-calibrated distances. We used the HPs formalism for joint analyses of the data sets to constrain the cosmological parameters  $h$  and  $\Omega_m$  (assuming a flat universe) and to check the reliability of the data sets.

Using the baryon mass fraction in clusters, we obtained a very high best fit for  $h$ . However, Figure 3 shows a strong correlation between  $h$  with  $\Omega_m$ ,  $\Omega_m h^{0.5} \approx 0.25$ . The addition of the cepheid sample to the cluster data changed significantly the best fit values,  $h = 0.72$  and  $\Omega = 0.26$ . This is not surprising, as the accurate cepheid-calibrated distances dominate the joint likelihood.

Recently, Douspis *et. al* (2001) combined CMB data with a fixed value for baryon fraction  $f_b = 0.048h^{-1.5} + 0.014$  and found  $\Omega_m \approx 0.4$ ,  $h \approx 0.6$ . Their results are in agreement with our derived combination,  $\Omega_m h^{0.5} \approx 0.25$  and in marginal agreement with our best fit values for  $\Omega_m$  and  $h$ , derived from the joint analysis of baryon fraction and the cepheid data. Our analysis differs from theirs in the sense that we have used individual gas fraction values for each of the 80 clusters in our sample, allowing self-consistency for the dependence of the gas fraction on  $\Omega_m$ .

More recently, Allen *et. al* (2002) used gas mass fraction measurements of 6 relaxed clusters observed with the Chandra Observatory, the HST Key Project value for  $H_0$  and the Big-Bang nucleosynthesis value for  $\Omega_b h^2$  to constrain  $\Omega_m$  and  $\Omega_\Lambda$ . The value they obtain for  $\Omega_m$  is again in very good agreement with our results.

In our analysis, we have found that HPs assigned to the cluster samples are lower than the values assigned to cepheid-calibrated distances. Indeed, it is worth noticing that some systematic uncertainties affect  $f_{\text{gas}}$  when it is estimated under the assumption of an isothermal gas in hydrostatic equilibrium with the dark matter gravitational potential, like in this paper. Some aspects of the physics of the ICM still need further understanding (e.g. the measurement of the total mass changes in presence of a gradient in the temperature profile and/or supporting pressure from non thermal component) and will be addressed in the near future with the

current X-ray missions Chandra (Weisskopf *et al.* 2000) and XMM-Newton (Hasinger *et al.* 2001). Moreover, we have not taken into account all contribution from baryons in dark matter to the cluster baryon budget.

There are also significant systematic uncertainties in the HST Key Project Result which should be addressed in the future. These uncertainties, discussed in detail in F01, are mainly due to the errors in the adopted distance modulus to the Large Magellanic Cloud (LMC) upon which the Cepheid period-luminosity relation is strongly dependent. Furthermore, the effects of reddening and metallicity on the Cepheid period-luminosity relation maybe stronger than expected (Shanks *et al.* 2002). It is also worth noting that the local variations in the expansion rate due to large scale velocities may effect the accurate determination of  $H_0$  (eg. Turner, Cen & Ostriker 1992).

Although our analysis is free of assumptions about the power spectrum of fluctuations, the results we obtain are in remarkable agreement with the  $\Lambda$ -Cold Dark Matter ‘concordance’ parameters (e.g Figure 5) derived from the Cosmic Microwave Background anisotropies combined with Supernovae Ia, 2dF galaxy redshift survey and other probes.

## ACKNOWLEDGEMENTS

We thank Steve Allen, Sarah Bridle, Wendy Freedman, Jeremy Mould and Jerry Ostriker for their helpful comments. PE acknowledges support from the Middle East Technical University, Ankara, Turkey, the Turkish Higher Education Council and Overseas Research Trust.

## REFERENCES

- Allen S.W., Schmidt R.W., Fabian A.C., 2002, MNRAS, 334, L11  
 Bahcall, N.A., Ostriker, J.P., Perlmutter, S., Steinhardt, P.J., 1999, Science, 284, 148  
 Bahcall, N.A., Comerford J.M., 2002, ApJ, 565, 5  
 Bridle, S.L., Eke, V.R., Lahav, O., Lasenby, A.N., Hobson, M.P., Cole, S., Frenk, C.S., & Henry, J.P. 1999, MNRAS, 310, 565  
 Bridle S.L., 2000, PhD thesis, University of Cambridge  
 Bridle S.L., Zehavi I., Dekel A., Lahav O., Lasenby A.N., Hobson M.P., 2001a, MNRAS, 321, 333  
 Bridle, S.L., Crittenden R., Melchiorri A., Hobson M.P., Kneissl R., Lasenby A.N., 2002, MNRAS, 335, 1193  
 Burles S., Nollett K.M., Turner M.S., 2001, ApJ, 552, L1-L6  
 de Bernardis P. *et al.*, 2002, ApJ, 564, 559  
 Douspis M., Blanchard A., Sadat R., Barlett J.G., Le Dour M., 2001, A&A 379, 1  
 Efron B., 1982, *The jackknife, the bootstrap and other resampling plans* Regional Conference Series in Applied Mathematics, no. 38, SIAM  
 Efstathiou G., Bridle S. L., Lasenby A. N., Hobson M. P., Ellis R. S. 1999, MNRAS, 303, L47  
 Efstathiou G. & 2dFGRS team, 2002, MNRAS, 330, 29  
 Eisenstein, D.J., Hu, W., Tegmark, M., 1999, ApJ, 518, 2  
 Ettori S., Fabian A.C., 1999, MNRAS 305, 834 (EF99)  
 Ettori S., Allen S.W., Fabian A.C., 2001, MNRAS, 322, 187  
 Ettori S., 2001, MNRAS, 323, L1  
 Evrard A.E., Metzler C.A., Navarro J.F., 1996, ApJ, 469, 494  
 Freedman, W.L., *et al.*, 2001, ApJ, 553, 47  
 Fukugita M., Hogan C.J., Peebles P.J.E., 1998, ApJ 503, 518  
 Gawiser E., Silk J., 1998, Science, 280, 1405  
 Hasinger G. *et al.*, 2001, A&A, 365, 45  
 Henry J.P., 2000, ApJ 545, 565  
 Hobson M.P., Bridle S.L., Lahav O., 2002, MNRAS, 335, 377  
 Kitayama T., Suto Y., 1996, ApJ 469, 480  
 Knox L., Christensen N., Skordis C., 2001, ApJ, 563, 95  
 Lahav, O., Bridle, S.L., Hobson, M.P., Lasenby, A.L., Sodré, L. 2000, MNRAS, 315, 45  
 Lahav, O., 2001a, in the proceedings of IAU201 *New Cosmological Data and the Values of the Fundamental Parameters* Manchester 2001, Eds. A. Lasenby and A. Wilkinson, in press, (astro-ph/0012475)  
 Lahav, O., 2001b, in the proceedings of *Astrophysical Ages and Time Scales*, Hawaii 2001, ASP conference series, pg. 617, Eds. T. von Hippel, C. Simpson and N. Manset (astro-ph/0105352)  
 Lahav O. & 2dFGRS team, 2002, MNRAS, 333, 961  
 Lineweaver C. H. 1998, ApJ, 505, L69  
 Mohr J.J., Mathiesen B., Evrard A.E., 1999, ApJ, 517, 627 (MME99)  
 Netterfield C.B., *et al.*, 2002, ApJ, 571, 604  
 Percival, J.W. & the 2dFGRS team, 2001, MNRAS, 327, 1297  
 Press, W.H., 1996, in *Unresolved Problems in Astrophysics*, Proceedings of Conference in Honor of John Bahcall, ed. J.P. Ostriker, Princeton: Princeton University Press (astro-ph/9604126)  
 Pryke C., Halverson N.W., Leitch E.M., Kovac J., Carlstrom J.E., Holzapfel W.L., Dragovan M., 2002, ApJ, 568, 46  
 Shanks T., Allen P.D., Hoyle F., Tanvir N.V., 2002, in *A New Era in Cosmology*, Eds. Metcalfe N., Shanks T., ASP Conf Ser, in press, (astro-ph/0208237)  
 Steigman G., Hata N., Felten J.E. 1999, ApJ, 510, 564S  
 Turner E.L., Cen R., Ostriker J., 1992, ApJ, 103, 1427  
 Wang L., Caldwell R. R., Ostriker J.P., Steinhardt, 1999, ApJ, 530, 17  
 Webster, M., Bridle, S.L., Hobson, M.P., Lasenby, A.N., Lahav, O., & Rocha, G. 1998, ApJ Lett, 509, L65  
 Weisskopf M.C., Tanabaum H.D., Van Spebroeck L.P., O’ Dell S.L., 2000, Proc SPIE 4012,2 (astro-ph/0004127)  
 White S.D.M., Navarro J.F., Evrard A.E., Frenk C.S., 1993, Nature 366, 429

## APPENDIX A: ESTIMATION OF THE GAS FRACTION

For an isothermal plasma in hydrostatic equilibrium, the gas mass fraction,  $f_{\text{gas}}$ , is calculated as the ratio of the mass of the gas and of the total gravitating mass,  $M_{\text{grav}}$ , within the radius,  $R_\Delta$ , at which the given mean overdensity of the total mass within cluster,  $\Delta$ , with respect to the background value,  $\Omega_m \rho_c$ , is reached:

$$f_{\text{gas}} = \frac{M_{\text{gas}}(< R_\Delta)}{M_{\text{grav}}(< R_\Delta)} = \frac{4\pi \int_0^{R_\Delta} \rho_{\text{gas}}(r) r^2 dr}{\frac{k T_{\text{gas}} R_\Delta}{G \mu m_p} \left( -\frac{\partial \ln \rho_{\text{gas}}}{\partial \ln r} \right)_{r=R_\Delta}}, \quad (\text{A1})$$

where  $R_\Delta = \theta d_{\text{ang}}$  is the physical radius,  $\theta$  is the angular separation,  $d_{\text{ang}}$  is the angular diameter distance,  $T_{\text{gas}}$  is the ICM temperature,  $k$  is the Boltzmann constant,  $\mu$  is the mean molecular weight in a.m.u. ( $\sim 0.6$ ),  $G$  is the gravitational constant and  $m_p$  is the proton mass.

The surface brightness,  $S(\theta)$  is given by the integral along the line of sight:

$$S(\theta) \propto \int \rho_{\text{gas}}^2 T_{\text{gas}}^{0.5} dl. \quad (\text{A2})$$

Hence, the gas density,  $\rho_{\text{gas}}$  is proportional to  $d_{\text{ang}}^{-0.5}$ . Combining this with the other dependence in Eq. A1,

$$f_{\text{gas}} \propto \frac{d_{\text{ang}}^{3-0.5}}{d_{\text{ang}}} = d_{\text{ang}}^{1.5} \propto h^{-1.5}. \quad (\text{A3})$$

For  $\Omega_k = 0$ ,  $d_{\text{ang}}$  can be written as

$$d_{\text{ang}} = \frac{c}{H_0(1+z)} \cdot \begin{cases} z & \text{if } \Omega_m = 0 \\ \int_0^z \frac{\Omega_m^{-1/2} d\zeta}{[(1+\zeta)^3 + \Omega_m^{-1} - 1]^{1/2}} & \text{otherwise} \end{cases} \quad (\text{A4})$$

The mean overdensity,  $\Delta$ , for  $\Omega_k = 0$  is given by (e.g. Kitayama & Suto 1996; Henry 2000)

$$\Delta(\Omega_m, z) = \Delta(\Omega_m = 1) \cdot \left[ 1 + 0.4093 (\Omega_{m,z}^{-1} - 1)^{0.9052} \right], \quad (\text{A5})$$

where  $(\Omega_{m,z}^{-1} - 1) = (\Omega_m^{-1} - 1)/(1 + z)^3$ .

The observed mass profile is calculated as

$$M_{\text{grav}}(< R_\Delta) = (4/3)\pi R_\Delta^3 \Omega_m \rho_c (1 + z)^3 \Delta \quad (\text{A6})$$

and is proportional to  $R_\Delta$  for a virialised system so that

$$R_\Delta \propto (\Omega_m \Delta)^{-0.5}. \quad (\text{A7})$$

## APPENDIX B: HYPER-PARAMETERS

Lahav *et al.* (2000) (see also Bridle 2000, Lahav 2001a & 2001b), generalised the standard procedure of combining likelihoods using the 'Hyper-Parameters' approach. The conventional way of combining likelihood functions of different data sets is either to give all the sets the same statistical weight or to assign weights in an ad-hoc way. The 'Hyper-Parameters' method generalises this approach by assigning each data a relative weight.

Given two independent data sets  $D_A$  and  $D_B$  (with  $N_A$  and  $N_B$  data points respectively), our approach is to combine the  $\chi^2$ 's in the following manner:

$$\chi_{\text{joint}}^2 = \alpha \chi_A^2 + \beta \chi_B^2, \quad (\text{B1})$$

where  $\alpha$  and  $\beta$  are 'Hyper-Parameters' (HPs). The maximum likelihood of a given model is estimated by minimising the above quantity. We calculate the  $\chi^2$ 's using the equation below:

$$\chi^2 = \sum \frac{1}{\sigma_i^2} [x_{\text{obs},i} - x_{\text{pred},i}(\mathbf{w})]^2 \quad (\text{B2})$$

where the sum is over the number of measurements,  $\sigma_i$  is the error for each data point and  $\mathbf{w}$  is the vector of free parameters we wish to determine (e.g.  $\Omega_m$  and  $h$ ).

The HPs are eliminated by marginalisation over  $\alpha$  and  $\beta$ :

$$P(\mathbf{w}|D_A, D_B) = \int \int P(\mathbf{w}, \alpha, \beta | D_A, D_B) d\alpha d\beta. \quad (\text{B3})$$

In order to evaluate the above integral, we use Bayes' theorem to write the following relations:

$$P(\mathbf{w}, \alpha, \beta | D_A, D_B) = \frac{P(D_A, D_B | \mathbf{w}, \alpha, \beta) P(\mathbf{w}, \alpha, \beta)}{P(D_A, D_B)}, \quad (\text{B4})$$

and

$$P(\mathbf{w}, \alpha, \beta) = P(\mathbf{w} | \alpha, \beta) P(\alpha, \beta). \quad (\text{B5})$$

We also assume the following:

$$P(D_A, D_B | \mathbf{w}, \alpha, \beta) = P(D_A | \mathbf{w}, \alpha) P(D_B | \mathbf{w}, \beta), \quad (\text{B6})$$

$$P(\mathbf{w} | \alpha, \beta) = \text{const.}, \quad (\text{B7})$$

and

$$P(\alpha, \beta) = P(\alpha) P(\beta). \quad (\text{B8})$$

We take the prior probabilities in Eq. B8 as Jeffreys' uniform priors in the log,  $P(\ln \alpha) = P(\ln \beta) = 1$ . Assuming Gaussianity, we write  $P(D_A | \mathbf{w}, \alpha) \propto \alpha^{N_A/2} \exp(-\frac{\alpha}{2} \chi_A^2)$  and similarly for  $D_B$ . It then follows that the probability for the parameters  $\mathbf{w}$  given the data sets is:

$$-2 \ln P(\mathbf{w} | D_A, D_B) = N_A \ln(\chi_A^2) + N_B \ln(\chi_B^2). \quad (\text{B9})$$

To find the best fit parameters  $\mathbf{w}$  requires us to minimise the above probability in the  $\mathbf{w}$  space. It is as easy to calculate this statistic as the standard  $\chi^2$ , and it can be generalized for any number of data sets.

Since  $\alpha$  and  $\beta$  have been eliminated from the analysis by marginalisation they do not have particular values that can be quoted. Rather, each value of  $\alpha$  and  $\beta$  has been considered and weighted according to the probability of the data given the model. It can be shown that the 'weights' are  $\alpha_{\text{eff}} = \frac{N_A}{\chi_A^2}$  and  $\beta_{\text{eff}} = \frac{N_B}{\chi_B^2}$ , both evaluated at the joint peak.